https://dx.doi.org/10.1016/j.conbuildmat.2023.132638


# Virtual-specimen modeling of aggregate contact effects on asphalt concrete

Zhifei Tan[a], Denis Jelagin[b], Hassan Fadil[b], Zhen Leng[a*], Rui Li[a,c], Jiwang Jiang[a], Peng Cao[d]

[a] Department of Civil and Environmental Engineering, The Hong Kong Polytechnic University, Hong Kong SAR, China

[b] Department of Civil and Architectural Engineering, KTH – Royal Institute of Technology, Brinellvägen 23, 10044, Stockholm, Sweden

[c] National & Local Joint Engineering Laboratory of Transportation and Civil Engineering Materials, Chongqing Jiaotong University, Chongqing, China

[d] College of Architecture and Civil Engineering, Beijing University of Technology, Beijing, China

Corresponding author:

Zhen Leng, Department of Civil and Environmental Engineering, The Hong Kong Polytechnic University, Hung Hom, Kowloon, Hong Kong

Email: zhen.leng@polyu.edu.hk

**Abstract**

Aggregate contacts may significantly affect the mechanical behavior of asphalt concrete, but there still lacks an effective way to account for them in numerical modeling. To address this demand, a new virtual-specimen modeling approach was developed in this study by simplifying aggregate particles in asphalt concrete as spheres and incorporating aggregate contacts through contact region (CR) elements. The complex moduli of both gap-graded and dense-graded mixtures were predicted using this approach, and compared with those predicted using the conventional image-based modeling approach and laboratory-measured values. The virtual-specimen modeling revealed that the CR in the gap-graded mixture with more large aggregates can better transmit load among aggregates than that in the dense-graded mixture. Both modeling approaches were found to provide good prediction accuracy, but the stress distributions in the virtual-specimen models were more uniform and continuous, leading to better computational convergence and the possibility of nonlinear analysis of asphalt concrete.

**Keywords**: Asphalt concrete; micromechanical modeling; aggregate contact; complex modulus

# 1 Introduction

Due to the high aggregate volumetric percentage in asphalt concrete, the interactions of the contacting aggregate particles significantly affect the mechanical performance of asphalt concrete [1, 2]. In many previous studies, the characteristics of aggregate contacts, in terms of their spatial distribution, orientation, etc., were found to affect the asphalt concrete mechanical performance profoundly. In particular, the effect of aggregate contacts on asphalt concrete's rutting resistance has been evaluated through image analysis of its microstructure [3, 4]. It was concluded that a better contact structure provides the mixture with better rutting resistance. Besides, micromechanical models based on homogenization theory were also developed and applied, which indicated that the conventional micromechanical models always predict underestimated dynamic moduli of asphalt concrete at low frequencies, but by considering the contacts between aggregates, the prediction can be significantly improved [5-7]. Accordingly, qualitative and quantitative understanding of how the contact interactions in aggregate skeleton affect its micro- and macro-mechanical behavior has become an important issue for both asphalt concrete's material design optimization and performance prediction. This study aims to contribute to this important topic by developing a computationally efficient approach for micromechanical modeling of asphalt mixtures which can account for aggregate contacts.

Recently, some attempts to consider aggregate contacts in numerical modeling have been made. One approach is to use the discrete element method (DEM), where the contact interactions between particles are defined explicitly [8, 9]. The DEM is an optimal simulation tool for particle materials, where the contact interactions define fully macro-scale mechanical behavior, such as loose asphalt mixture [10-12]. However, capturing the complicated rheological behavior of the compacted asphalt mixtures is problematic in the DEM simulations, as the load between the adjacent aggregate particles is also transferred through the binder phase. Micromechanical finite element (FE) modeling is a promising alternative in this context. However, explicit modeling of the aggregate contacts in the micro-mechanical models of asphalt concrete is extremely computationally expensive, which precludes the analysis on practically relevant scales. In a recent study, Ling and Bahia [13] developed 2D FE models to simulate the effect of aggregate contact on rutting. In this study, the effect of aggregate contacts was accounted for indirectly by modifying the properties of the binder film between the adjacent aggregates to the aggregates' properties. It was found that accounting for aggregate contacts substantially improved the modeling predictions of asphalt concrete's performance in the flow number test. Tan et al. [14] proposed an approach to consider aggregate contacts in 3D FE models. In this approach, the microstructural model of asphalt concrete was generated from X-ray computed tomography (CT) measurements, and aggregate contacts were identified based on the surface distance threshold (SDT) concept proposed by [15, 16], where SDT is defined as the surface distance between two neighboring aggregates. If the distance is smaller than the SDT value, the two aggregates are considered to be in contact. Tan, et al. [14] introduced the contact regions (CR), or contact zones, between the identified aggregate contact pairs in numerical modeling, which showed that incorporating CR improves the prediction accuracy of the viscoelastic properties of asphalt concrete at low loading frequencies.

In many previous studies, the 3D FE microstructural model was generated from X-ray CT measurements [17-19]. Although CT-based modeling can capture realistic internal structures of the materials, it has several obvious drawbacks. First, the highly irregular surfaces in CT datasets tend to result in FE models with an extremely large number of elements and, accordingly, very high computational costs. Hence, a CT-based approach can only be used for modeling relatively small material volumes. Second, the high cost of CT scanning makes it impossible to generate many models and developing micromechanical models with target volumetrics is impossible [20]. One promising alternative is micromechanical modeling based on simplified computer-generated internal structures. Fadil et al. [21, 22] proposed an approach for micromechanical modeling of binder-aggregate composites based on computer-generated internal structures, which has been successfully applied to evaluate the viscoelastic behavior of asphalt mastic and mortar. It was reported that the use of simplified computer-generated internal structures significantly reduces the model computational cost, thus allowing for micromechanical modeling of relatively large-scale processes, such as the indentation test on asphalt mortar. However, such an approach has neither been applied to study the binder-aggregate composites with coarse aggregates such as asphalt concrete, nor the effects of stone-to-stone contacts. These gaps will be addressed in the present study by developing virtual-specimen micromechanics models incorporated with CR.

In order to achieve computational efficiency, the proposed virtual-specimen approach is developed based on computer-generated simplified microstructures of asphalt concrete. In this simplification, the asphalt concrete is modeled to have three phases, including viscoelastic matrix, embedded spherical elastic aggregates, and air voids. In addition, CR elements are introduced between adjacent aggregates. With the proposed modeling approach, the mechanical behaviors of two common types of asphalt mixtures are examined. The model's capability to capture the effective complex modulus of the two asphalt mixtures is verified by comparing the model-predicted and lab-measured complex moduli. The effect of the simplified microstructure on the predicted local stress distribution is also examined by comparing the results against those from the CT-based models. Finally, the developed asphalt concrete models are employed to understand how the CR characteristics affect the dynamic response of asphalt concrete under loading.

## 2 Problem formulation and micromechanical model development

Asphalt mixtures are composite materials consisting of at least three phases: elastic aggregates, viscoelastic binder, and air voids. The sizes of aggregates in asphalt concrete vary in a wide range from micrometers to millimeters [23]. Thus, explicitly incorporating the full gradation curve into the micromechanical modeling of asphalt concrete is extremely computationally intensive [24]. A common approach to overcome this difficulty is to employ a multiscale approach, where, at asphalt concrete scale, only aggregates larger than a certain size are modeled explicitly [25-27]. The viscoelastic matrix, known as fine aggregate matrix (FAM) or asphalt mortar, represents a mixture of bitumen, mineral filler, and fine aggregates [14, 28]. The effective viscoelastic properties of the matrix phase may be determined from the

experiments [14] or the models at smaller length scales [21]. In the modeling approach proposed in this study, asphalt mixtures are modeled as aggregates, larger than the maximum aggregates in FAM, embedded in FAM - a continuous material consisting of bitumen and small aggregates. At small strains or in the absence of damage, FAM can be described as a linear viscoelastic material, with their constitutive relationship defined as [29]:

$$\sigma(t) = \int_0^t G(t-\tau)\frac{d\varepsilon(\tau)}{d\tau}d\tau \quad (1)$$

where $t$ is time; $\tau$ is a time variable of integration; and $G(t)$ is the relaxation modulus in shear. The Prony series model, also called the generalized Maxwell model, is used to describe the shear relaxation function of FAM as follows [29]:

$$G(t) = G_0[1 - \sum_{i=1}^{n} g_i(1 - e^{-t/\tau_i})] \quad (2)$$

where $g_i = \frac{G_i}{G_0}$; $G_0$ is the instantaneous shear modulus; $G_i$ and $\tau_i$ are the shear modulus and relaxation time for the $i$'s element; and $n$ is the number of Maxwell elements used to fit the equation. Through Fourier transform, the Prony series terms in the time domain can be transformed to the frequency domain as shown below [29]:

$$G'(\omega) = G_0[1 - \sum_{i=1}^{n} g_i] + G_0 \sum_{i=1}^{n} \frac{g_i\tau_i{}^2\omega^2}{1+\tau_i{}^2\omega^2} \quad (3)$$

$$G^{"}(\omega) = G_0 \sum_{i=1}^{n} \frac{g_i\tau_i\omega}{1+\tau_i{}^2\omega^2} \quad (4)$$

$$G^*(\omega) = G'(\omega) + iG''(\omega) \quad (5)$$

where $G^*$, $G'$and $G''$ denote the complex, storge and loss moduli, respectively; $\omega$ is the angular frequency. In this study, it is assumed that the Poisson's ratio of FAM is 0.4, while $G^*(\omega)$ is measured experimentally, as described in Section 4.

An adequate representation of the internal structure and volumetrics of asphalt concrete is essential for ensuring accurate modeling results, which can be achieved based on CT measurements combined with image analysis techniques [14, 18]. However, the models generated from X-ray CT data are often too complicated for numerical modeling on large scales and/or with nonlinear material behavior considered. Hence, this study proposes a simplified approach for asphalt concrete's micromechanical modeling based on computer-generated internal structures. The effects of aggregate contacts are incorporated into the model through CR elements, following the method proposed by Tan, et al. [14]. For comparison, micromechanical models for the same asphalt mixtures are also generated based on their internal structures obtained from CT measurements. In this paper, the models with the computer-generated and CT-based internal structures are referred to as "virtual-specimen model" and "CT model", respectively. The procedures for generating the virtual-specimen and CT models are elaborated in Sections 2.1 and 2.2, respectively.

## 2.1 Virtual-specimen model

Figure 1 presents the process of the microstructural model generation proposed in this study. In the model, the aggregate particles are represented by spheres with their sizes following asphalt mixture's aggregate gradation. In the first step, the microstructure of asphalt concrete is generated using the LAMMPS software. In this step, spherical particles are randomly generated in a cubic container of 80mm*80mm*100mm. The particle diameters are enlarged by 5% of their gradation sizes to avoid overlapping between the neighboring aggregates. After that, particles are allowed to drop under gravity and then compacted to the design height of 80 mm, as shown in Figure 1(a). In the next step, based on the coordinate information and particle diameters, the developed microstructural model in LAMMPS is regenerated into ABAQUS through a developed Python script. The real particle diameters are assigned to regenerate the model with actual sizes. By cutting, assembling, and meshing, four cylindrical specimens with 25 mm diameter and height are generated, as presented in Figure 1(b).

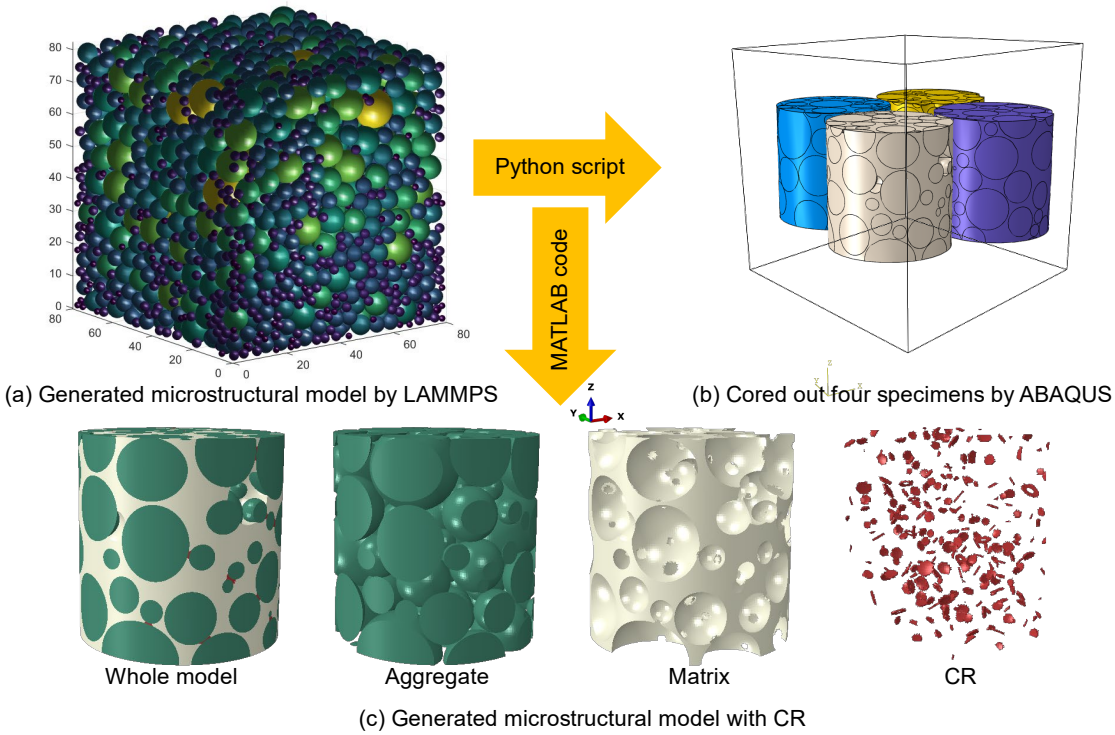


Figure 1 Virtual-specimen model generation

In the final step, the CR in the FE model is identified. As discussed in the reference [14], CR only occupies a tiny portion of asphalt concrete, but its effects on the stress transmission between aggregate and the mechanical performance of asphalt concrete are significant. Therefore, CR should also be considered as a phase and incorporated into the generated models. To find out the CR from the generated meshed model, MATLAB codes were developed. The program workflow is presented in Figure 2, and Figure 3 schematically illustrates how to search the CR elements. In these codes, the element ID (eleID), node coordinates (nodCor) and sphere radii (sphR), centre coordinates (sphCor) and SDT value are used as inputs. To reduce the search region for CR elements, the matrix elements surrounding the particles (eleSur) with a distance smaller than the defined SDT value are identified first as the potential CR elements, as shown in Figure 3(a). Besides, the minimum surface distance of each particle pair is calculated. If the

surface distance of the sphere pair is smaller than the given SDT value, the particle pair is identified as the potential contact spheres, as shown in Figure 3(b). Further, the distance from the potential CR elements of one sphere to another sphere's surfaces will be calculated. If the distance is smaller than the given SDT value, that element will be chosen as a CR element, as shown in Figure 3(c). The identified CR elements will be grouped as a CR element set in the input file of ABAQUS. By selecting different SDT values, models with different volumetric percentages of CR can be generated. It only takes several minutes to find out all CR elements for a model with millions of elements. Figure 1(c) presents the developed model with CR.

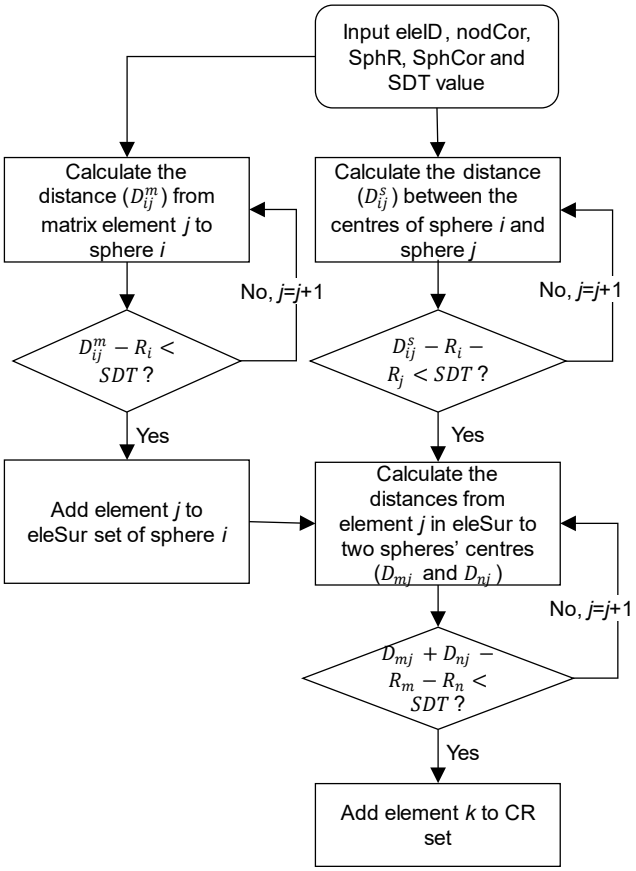


Figure 2 Flowchart of CR element searching

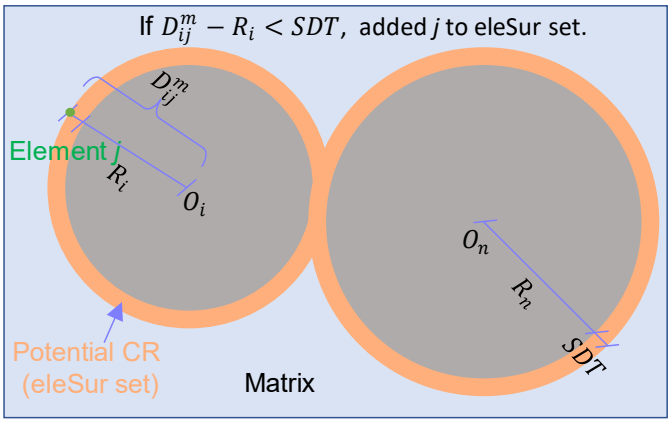


(a) Step 1: Identify the potential CR elements ( eleSur set)

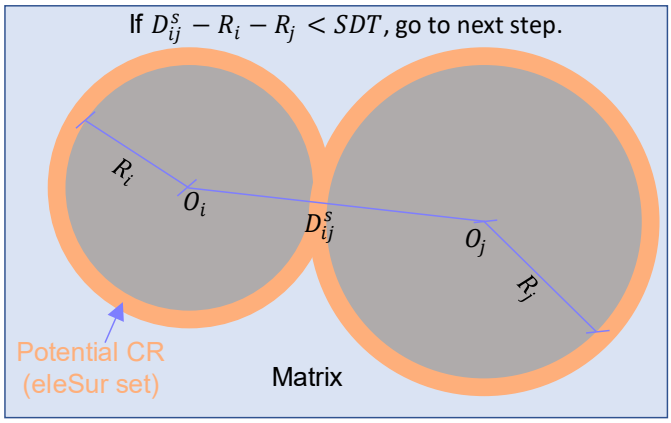


(b) Step 2: Identify the potential contact sphere pairs

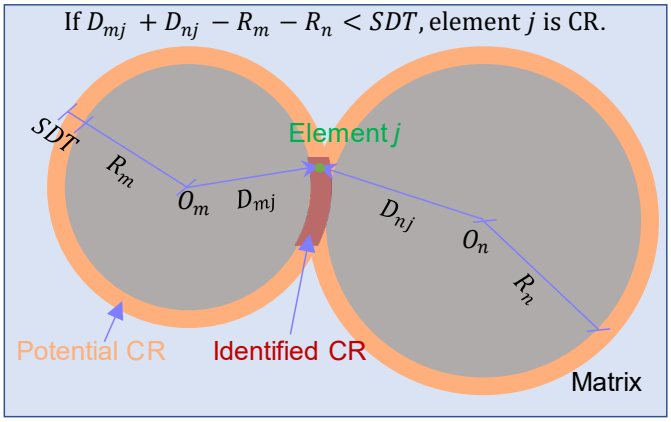


(c) Step 3: Identify the CR elements from the potential CR elements

Figure 3 Schematic diagram of CR element searching

### 2.2 CT-based model

CT-based models in this study are generated following the methodology proposed by Tan, et al. [14]. As shown in Figure 4, CT images are first segmented into three phases (matrix, aggregate, and air void) through digital image processing (DIP) techniques [30]. The flat field correction is used for background correction, the median filter is adopted to reduce image noise, and watershed algorithms are applied to image segmentation. Further, algorithms developed in previous studies are used to generate the images with CR [3, 4]. The algorithms can search around the peripheries of particles and then recognize the CR pixels based on the given SDT value. Finally, the images with CR are converted to meshed models using the advanced Delaunay-based mesh method [31]. Through this processing, a cubic meshed model with four phases, including matrix, aggregate, air void, and CR, can be developed.

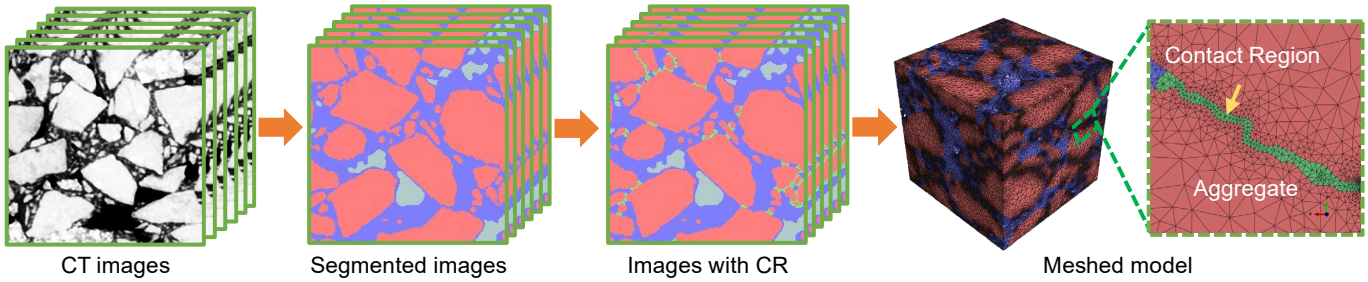


Figure 4 CT model generation

## 3 Computational study

The computational approaches outlined in the previous section are used in this study to develop the models for two asphalt mixtures commonly in Hong Kong, namely a stone mastic asphalt with a nominal maximum aggregate size (NMAS) of 10 mm (SMA10) and a dense-graded mixture with a NMAS of 10 mm (AC10). For each asphalt mixture, four cylindrical virtual specimens are cored out from the big cubic model, as shown in Figure 1(b). Besides, four SDT values, including 0.0, 0.1, 0.2, and 0.3 mm, are selected to consider CR in the virtual-specimen models. Therefore, a total of 32 virtual-specimen models are generated for the two mixtures. For simplicity, the generated virtual-specimen models are labeled in the format of "AC_type_specimen_No._SDT". For example, "SMA10_1_0.1" represents the first cylindrical specimen of SMA10 with CR at 0.1 mm SDT value. Figure 5 presents the two generated virtual-specimen models for both mixtures. It is interesting to notice that the dense-grade AC10 shows more small particles and smaller CRs than SMA10. The microstructural differences are expected to affect the macroscopic mechanical performances of both mixtures. For comparison, a CT-based model of SMA10 is also generated following the procedure summarized in Section 2.2. The cubic CT model with a length of 20 mm and CR at 0.1mm SDT value is labeled as SMA10_CT_0.1. The previous study proved that a 0.1 mm SDT value could incorporate all the CR into the CT image-based model [14].

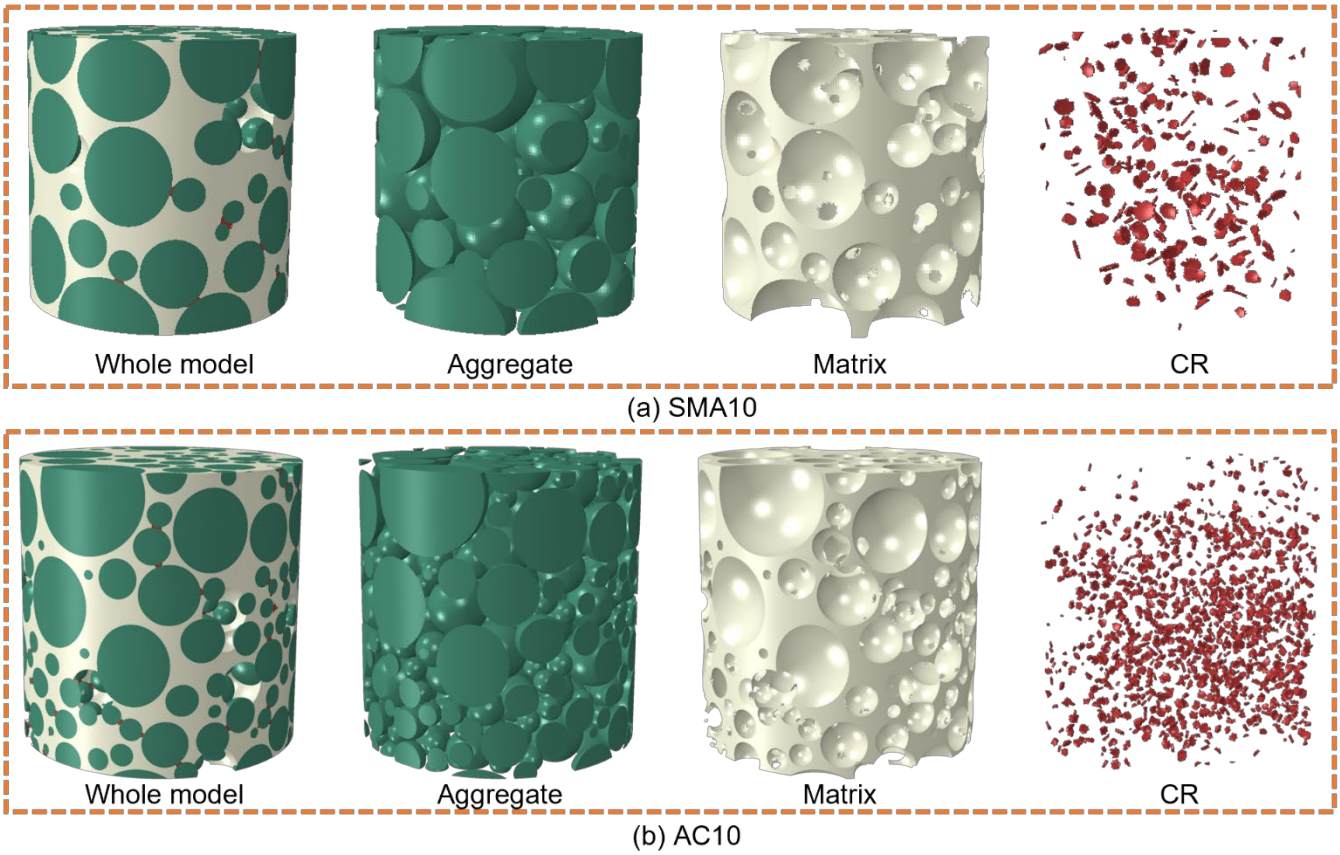


Figure 5 Examples of the developed SMA10 and WC10 models at SDT=0.2 mm

To characterize the volumetric properties of the generated virtual-specimen models, the volumetric compositions of the developed 32 virtual specimens are analyzed and listed in Table 1. Since at different SDT values, the aggregate and air voids are the same for the models with the same specimen ID, the compositions of aggregate, matrix, and air voids in the models without CR (SDT=0.0 mm) are presented, and only the CR volumetric percentages are listed for models at other SDT values. For comparison, the volumetric compositions of the CT-based model and the real asphalt mixtures are presented in Table 1 as well. It can be seen that the volumetric percentages of the aggregate, matrix and air void in the generated virtual-specimen models vary somewhat due to the random microstructure generation procedure. At the same time, the variabilities are pretty narrow, and the volumetric percentages of the generated models never deviate more than 4% from the target values. However, it is interesting to notice that at the same SDT value of 0.1 mm, the volumetric percentages of CR in the virtual-specimen models (0.04%) are much lower than in the SMA10_CT_0.1 model (1.9%). Even at a high SDT value of 0.3 mm, the volumetric percentages of CR in the virtual-specimen models are no more than 2% for both mixtures. Two reasons may cause this difference. On the one hand, due to the limited resolution of the CT image, the erosion of the aggregate periphery during segmentation may increase the volume of CR in the CT model. On the other hand, the lower surface-to-volume ratio of the sphere particles may lead to fewer aggregate contacts in the virtual-specimen model. Nevertheless, what can be confirmed is that CR only occupies a very tiny volumetric percentage in all models.

Table 1 Volumetric properties of virtual-specimen models, laboratory mixtures, and CT model (%)

| Specimen ID | Aggregate | Matrix | Air void | CR | | |
|---|---|---|---|---|---|---|
| | SDT=0.0 mm | | | SDT=0.1 mm | SDT=0.2 mm | SDT=0.3 mm |
| SMA10_1 | 65.46 | 31.25 | 3.29 | 0.04 | 0.28 | 0.74 |
| SMA10_2 | 64.82 | 32.46 | 2.73 | 0.04 | 0.29 | 0.78 |
| SMA10_3 | 67.83 | 30.14 | 2.03 | 0.04 | 0.30 | 0.82 |
| SMA10_4 | 63.72 | 32.11 | 4.17 | 0.04 | 0.32 | 0.85 |
| SMA10 mixture | 64.00 | 31.50 | 4.50 | - | - | - |
| SMA10_CT_0.1 | 63.80 | 31.30 | 4.90 | 1.90 | - | - |
| AC10_1 | 61.03 | 36.00 | 2.97 | 0.01 | 0.42 | 1.62 |
| AC10_2 | 64.75 | 32.68 | 2.56 | 0.01 | 0.22 | 0.94 |
| AC10_3 | 60.33 | 35.95 | 3.72 | 0.01 | 0.47 | 1.86 |
| AC10_4 | 63.15 | 33.53 | 3.32 | 0.01 | 0.36 | 1.47 |
| AC10 mixture | 62.04 | 34.46 | 3.50 | - | - | - |

Table 2 presents the material properties used in modeling. The granite aggregate is assumed to be elastic. Based on the aggregate gradations of both mixtures, the maximum FAM aggregate sizes of SMA10 and AC10 are 2.36 mm and 1.18 mm, respectively. The reason why a smaller maximum aggregate size is selected for the matrix of AC10 is that the aggregates from 1.18 mm to 2.36 mm also occupy a significant portion of AC10 (around 16% of the mixture volume). Thus, it may significantly affect the contact properties in the dense-graded mixture. It can be found that generated models for both mixtures have close aggregate volumetric percentages, as presented in Table 1 (64% and 62% for SMA10 and AC10, respectively). A constant Poisson's ratio of $\nu$=0.4 is assumed for FAM in this study [14]. The shear complex modulus for FAM is measured as detailed in the following section. The results are fitted with the Prony series, cf. equation (2), and the corresponding master curves of the Prony series model are plotted in Figure 7, which shows good fitness with the experimental master curves. Besides, the CR phase is also represented as a linear viscoelastic material, with its properties determined from FAM measurements and aggregate properties, following the procedure proposed in [14].

Table 2 Material properties

| Materials | Poisson's ratio | Elastic/ Complex Modulus |
|---|---|---|
| Aggregate | 0.2 | 60,000 MPa (Elastic) |
| FAM | 0.4 | Prony Series Model (Viscoelastic) |
| CR | 0.4 | Prony Series Model (Viscoelastic) |

Figure 6 presents the meshed models for both studied asphalt mixtures. In this study, the virtual-specimen models are meshed with linear tetrahedral elements (C3D4). Trial simulations are performed with mesh sizes of 0.15 mm and 0.25 mm, which results in a difference of less than 1.5%. Thus, 0.25 mm is selected as the mesh size. With such mesh size, the average element number for the virtual-specimen models

is around 1.70 million, while it is 6.26 million for the CT-based models. Thus, the simulation computation is significantly reduced, making it possible to model large material volumes and incorporate nonlinear effects into the analysis.

The steady-state dynamics (SSD) method is adopted to conduct the FE simulation [14, 32]. This method is based on the perturbation theory and performs the simulation at different loading frequencies, which makes it much more efficient than the conventional dynamic simulation method based on transient dynamics [32, 33]. A computer with a 2.8 GHz CPU is used. It takes approximately two hours for the CT-based models to compute the moduli of eleven frequency points from $10^{-6}$ Hz to $10^{4}$ Hz. In contrast, for the virtual-specimen models, it only takes less than one hour to complete the same simulation.


Figure 6 Examples of the meshed virtual-specimen models (Blue: aggregate phase; white: matrix phase; red: CR phase)

## 4 Experimental study

The viscoelastic properties of the FAMs and mixtures for both asphalt mixtures were measured. In this study, the granitic aggregates were used for both asphalt mixtures, i.e., SMA10 and AC10. The styrene-butadiene-styrene (SBS) modified binder with a Superpave performance grade of 76-16 (PG76-16) was used for SMA10, while the virgin asphalt binder with a penetration grade of 60/70 (Pen60/70) was utilized for AC10. Based on the mixture gradations, the corresponding compositions of FAM can be calculated based on the method proposed by Underwood and Kim [23]. The calculated binder contents for the FAMs of SMA10 and AC10 are 21.1% and 14.1%, respectively. Based on the compositions, the FAM materials and the specimens for testing can be fabricated following the method proposed in the previous studies [14, 28]. The dynamic shear rheometer (DSR) was used to measure the complex modulus. Frequency sweep tests at temperatures from -10 to 50°C and frequencies from 100 Hz to 0.1 Hz were performed on the prepared FAM specimens. Based on the measured moduli at different temperatures, the master curves of FAM at a wider frequency range can be constructed [28, 34]. After that, the viscoelastic properties of CR can also be determined from the measured viscoelastic properties of FAM and the elastic properties of aggregate following the procedure proposed by Tan, et al. [14]. Frequency sweep tests were also performed on the two asphalt mixtures in accordance with AASHTO T342, which are used to compare with the modeling results. For instance, Figure 7 presents the constructed master curves of FAM, CR, and asphalt concrete of SMA10.

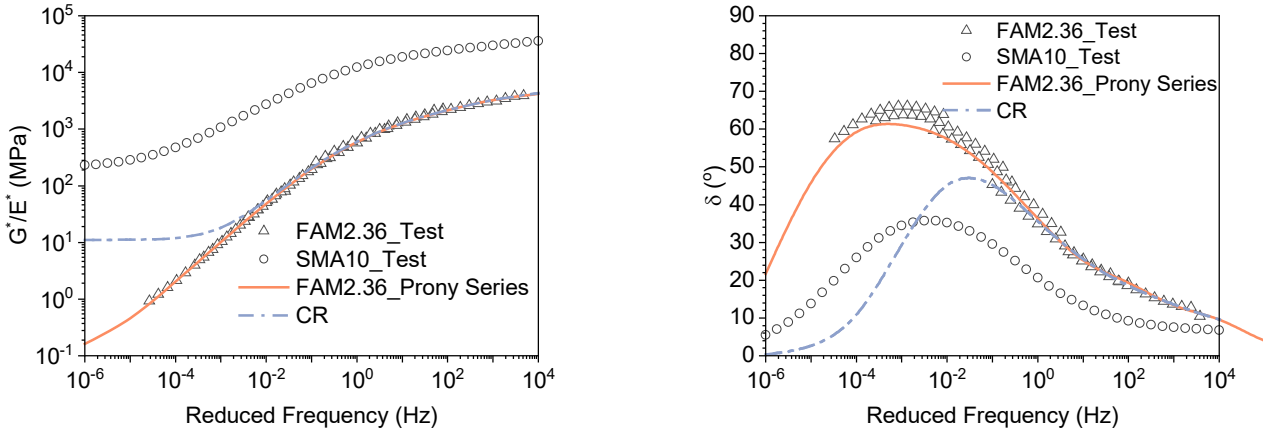


(a) Dynamic modulus (b) Phase angle

Figure 7 Master curves of measured FAM, fitted Prony series, CR, and measured asphalt concrete of SMA10 at a reference temperature of 10 °C

## 5 Results and discussion

In this section, the predicted master curves based on virtual-specimen and CT models are compared to evaluate whether the generated model based on the proposed method can capture the viscoelastic properties of asphalt concrete. After that, the stress distributions in both types of models are presented to characterize the effect of micromechanical characteristics on their internal stress. In the end, statistical analyses on the internal stresses in the three phases, including aggregate, matrix, and CR, are performed to identify the internal stress difference in different phases and the effect of SDT values.

### 5.1 Master curves

To evaluate the performance of the virtual-specimen modeling approach, the eight virtual-specimen models (four models for SMA10 and four models for AC10) with an SDT value of 0.1 mm are developed and applied to predict the mixtures' master curves, as shown in Figure 8. For comparison, the lab-measured master curves are also plotted. It can be seen that, for both asphalt mixtures, the four virtual-specimen models for each mixture provide similar predicted dynamic moduli and phase angles at different loading frequencies. However, compared with the experimental data, the virtual-specimen models significantly underpredict the dynamic moduli but overpredict the phase angles of both asphalt mixtures at frequencies lower than 0.01 Hz. It is believed that although the same 0.1 mm SDT value is used, the relatively lower volumetric percentages of CR in the virtual-specimen models, as shown in Table 1, reduce the aggregate contacts between particles, thus leading to the lower predicted moduli. To include enough aggregate contacts into the virtual-specimen model, a higher SDT value than the one used in the CT model should be selected. This is somewhat can be expected since at the same distance between two aggregates, irregular aggregates in asphalt concrete would have more interaction points compared with the idealized spherical particles in the virtual-specimen model. Therefore, the effect of SDT values on the prediction of the virtual-specimen model should be further investigated.

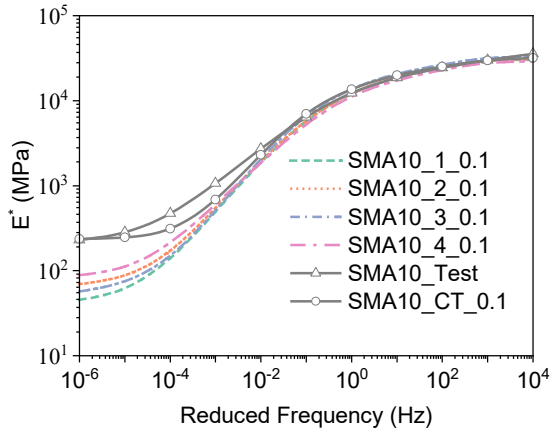


Dynamic modulus of SMA10

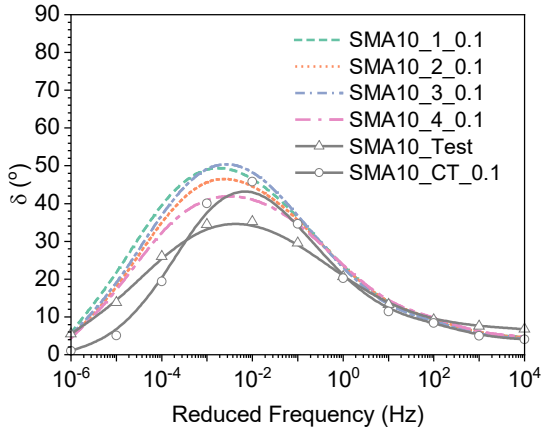


Phase angle of SMA10

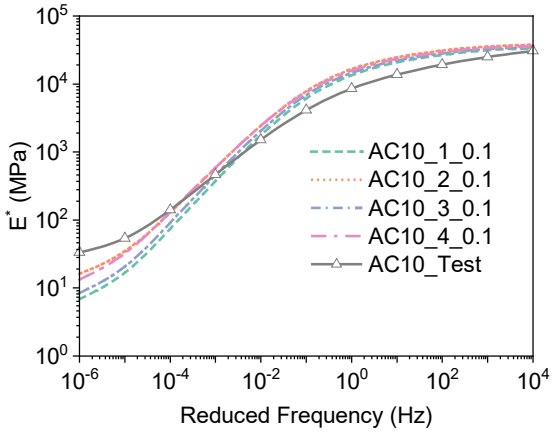


Dynamic modulus of AC10

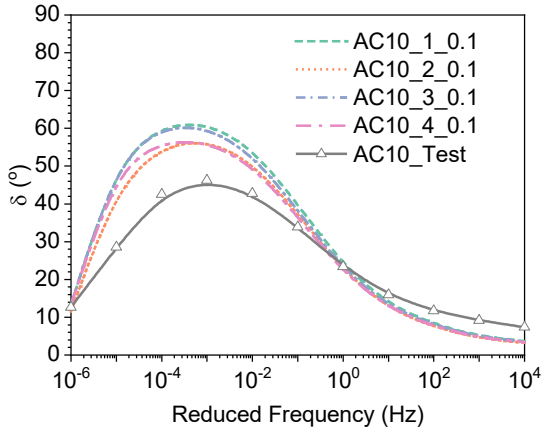


Phase angle of AC10

Figure 8 Predicted master curves of SMA10 and AC10 at 0.1 mm SDT value

Figure 9 shows the average master curves predicted by the virtual-specimen models at different SDT values (0.0, 0.1, 0.2, and 0.3 mm). Besides, the master curves of the CT image-based model and the experimental curves are also plotted. It can be found that with the increase of SDT value, the moduli at low frequencies increase for both mixtures. At an SDT value of 0.2 mm, the predicted average master curves can be significantly improved using the experimental curves as references. Besides, from Figure 9(a) and (b), it can be noticed that for SMA10, the virtual specimen model at SDT=0.2 and the SMA10_CT_0.1 model give almost identical prediction results. Thus, an equivalent SDT value of 0.2 mm is selected for the virtual-specimen model. Although the predicted results, especially the master curves, still have some differences compared to the experimental results, it is considered reasonable due to the anisotropic properties of CR, which will be studied in future research.

In addition, the effects of aggregate contacts on both mixtures can also be discovered in Figure 9. Although the increasing rate of dynamic moduli at low frequencies decreases with increasing SDT values for both asphalt mixtures, CR has more significant effects on SMA10 than AC10. Taking the result at $10^{-6}$ Hz as an example, comparing the predicted dynamic moduli by the virtual-specimen models at SDT=0.0 mm with SDT=0.2 mm, more than ten-time improvement can be found in SMA10, but only around a one-time increase in AC10. This result agrees with the microstructural properties in Figure 5. More small particles in AC10 make the CR too tiny and thus cannot develop force chains to effectively transmit stress among aggregate as SMA10.

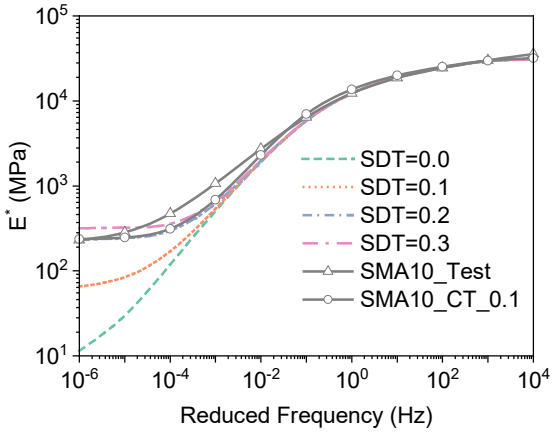


(a) Dynamic modulus of SMA10

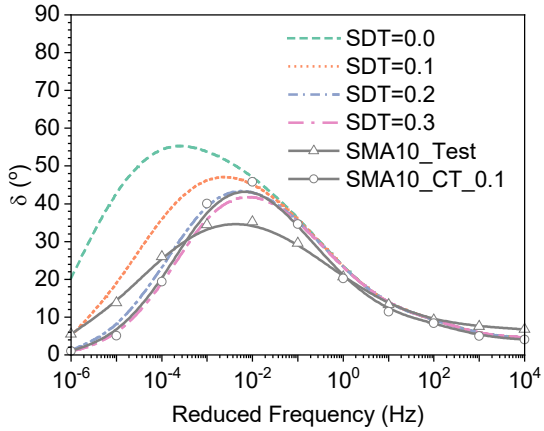


(b) Phase angle of SMA10

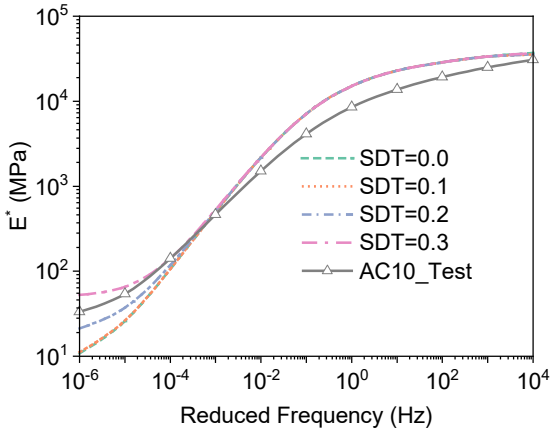


(c) Dynamic modulus of AC10

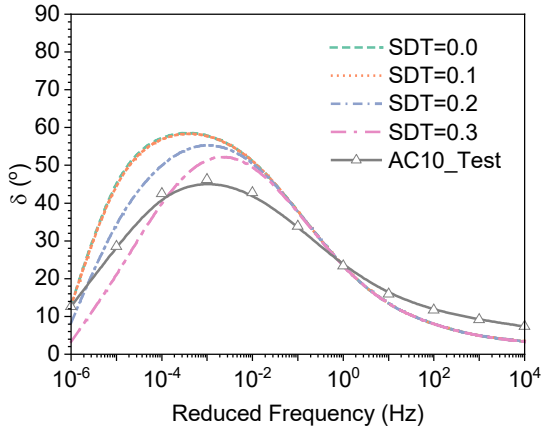


(d) Phase angle of AC10

Figure 9 Experimental master curves and the predicted average master curves by virtual-specimen models at different SDT values (0.0, 0.1 and 0.2, 0.3 mm) and CT model

### 5.2 Stress distribution

Figures 10(a)-(d) present the maximum principal stresses of the SMA10 and AC10 virtual-specimen models, respectively, at two frequencies: $10^{-6}$ Hz (representing a low loading frequency) and $10^{3}$ Hz (representing a high loading frequency). For comparison, the internal stress in the SMA_CT_0.1 model is also analyzed, as shown in Figures 10(e) and (f). The stress distributions in the three phases, including aggregate, matrix, and CR, are presented separately for the three models. From the three figures, it can be found that the stress distributions in the three models display similar characteristics. At a low frequency, the aggregate and CR phases show much higher stress than the matrix phase, which indicates that most of the stress in asphalt concrete transmit among the connecting aggregate particles via CR. In contrast, at the high frequency of $10^{3}$ Hz, the matrix phase also exhibits high stress, indicating that the matrix phase can also play an important role in stress transmission with increasing frequencies. This result agrees with the findings from the previous study [14]. The high stresses in all phases at the high frequency also explain that all the predicted master curves of the virtual-specimen models at different SDT values start to converge at high frequencies. The increasing domination of the matrix phase in the stress transmission dwarfs the effect of CR and thus leads to close predictions in complex moduli. Besides, comparing Figure 10(a) with Figure 10(c), it can be observed that at the low frequency, aggregate and CR phases in SMA10 show higher stresses

than AC10, which suggests that the CR in SMA10 can transmit the stress better than AC10 and thus develop stress chains. This explains why the dynamic modulus of SMA10 is much higher than AC10 at $10^{-6}$ Hz (more than four times). It also indicates that aggregate contacts have a more prominent influence in the gap-graded mixture than the dense-graded mixture.

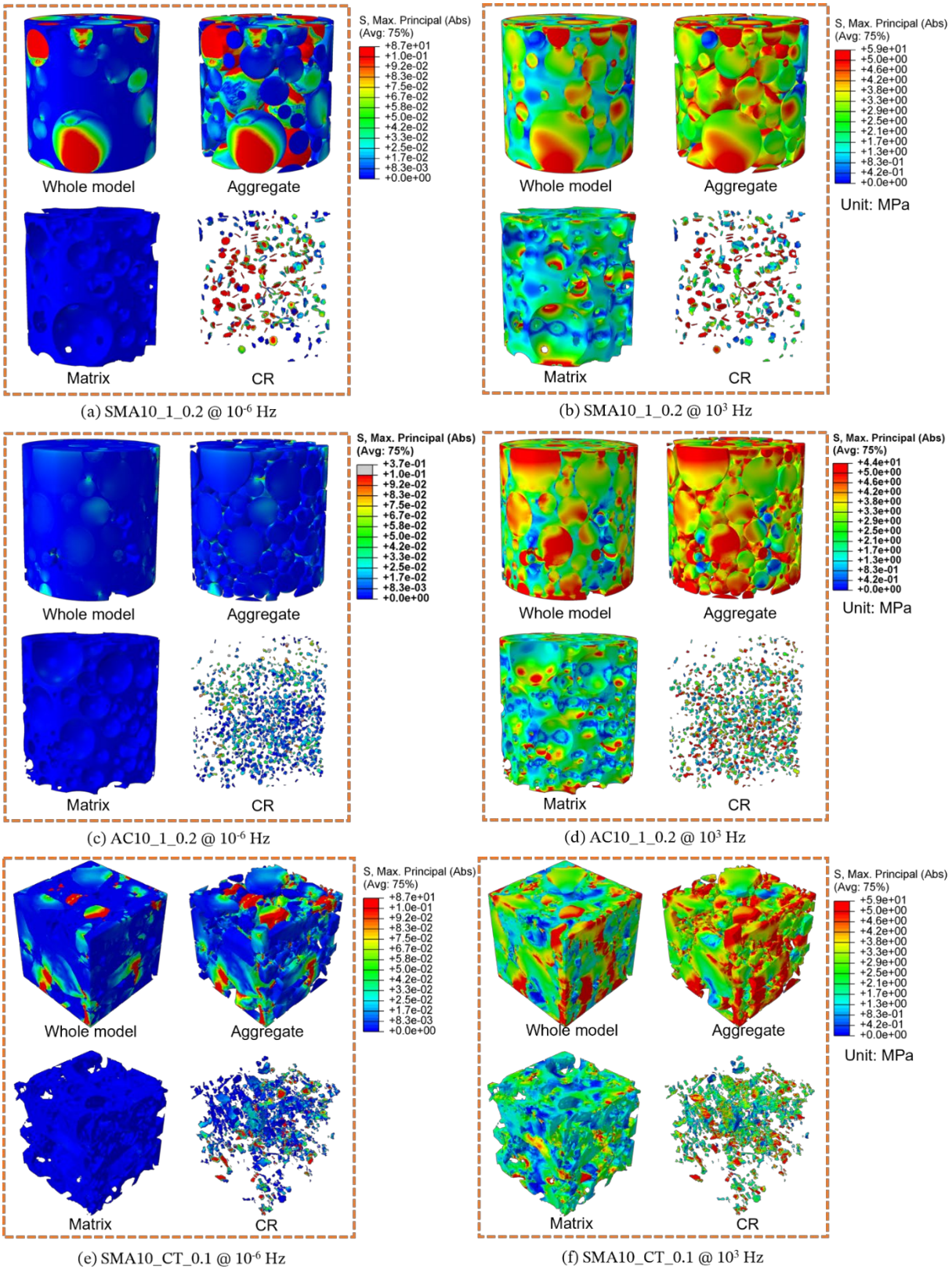


Figure 10 Maximum principal stress distributions in the virtual-specimen and CT models

In Figure 10, significant stress differences can be observed in different phases of asphalt concrete at $10^{-6}$ Hz. However, the stress distributions cannot show the detailed stress properties in the model. Hence,

statistical analysis of the stresses in different phases is conducted to understand the local mechanical properties further. Taking SMA10 as an example, the maximum principal stresses in the SMA10_CT_0.1 model and the virtual-specimen models of SMA10_1 at the four SDT values (five models in total) are evaluated to investigate the internal stress characteristics in the virtual-specimen model as well as the effect of SDT value on the internal stress. As presented in Figure 11, three statistical parameters, including the cumulative stress distribution, and the average and maximum stresses, are used to analyze the stress properties in the three phases, i.e., aggregate, matrix, and CR.

Firstly, to study the stress characteristics in the virtual-specimen model, it is necessary to compare the statistical results of the virtual-specimen models with the CT model. As concluded in the previous analysis, the virtual-specimen model at 0.2 mm SDT value is equivalent to the CT model at 0.1 mm SDT value. Therefore, the statistical results of SMA10_1_0.2 are compared with SMA10_CT_0.1. Figure 11(a), (c), and (e) present the cumulative distribution curves of aggregate, matrix, and CR phases, respectively. It can be found that the cumulative distribution curves of the SMA10_CT_0.1 model are on the left of the curves of the SMA10_1_0.2 model for all phases, indicating that the virtual-specimen model has a higher volumetric ratio of high stress than the CT model. Figure 11(b), (d), and (f) present the average and maximum stresses in the three phases of asphalt concrete. It can be noticed that in all three phases, the SMA10_1_0.2 model displays higher average stresses than the SMA10_CT_0.1 model, which is in agreement with the findings from the cumulative curves, but much lower maximum stresses. This result means that the stress distribution in the CT model is more heterogeneous than in the virtual-specimen model. Although the CT model's average stress is low, the high-stress points may dominate the stress transmission. This difference may be the reason why the CT_0.1 model has lower average stresses than the virtual-specimen models in all phases, but it still can give close predicted moduli to the virtual-specimen model. Besides, the much higher maximum stress in the CT_0.1 model also indicates that stress concentrations exist in the CT model, which can also be observed in Figure 10(e), where high-stress points can be observed in the aggregate and CR phases in the CT model. It is possible for the CT model with irregular aggregate particles to lead to high stress in the tip regions of particles. Unlike the CT model, the regular spherical particles in the virtual-specimen model make the stress distribution more continuous and uniform and thus smaller maximum stresses in virtual-specimen models, as presented in Figure 10(a). This characteristic is advantageous to the convergence of FE computation. However, it should also be noted that although the virtual-specimen model can well capture the macroscale properties of asphalt concrete, its uniform stress distribution characteristic may also imply that some local failure properties in asphalt concrete may be missed.

To evaluate how SDT values affect the internal stress of asphalt concrete, the internal stresses of the virtual-specimen models at the four SDT values are statistically analyzed. Figures 11(a) and (b) show that the high-stress volumetric ratio and average and maximum stresses in the aggregate phase increase with SDT values. These results can be expected since, with increasing SDT value, more CR can improve the

stress transmission between particles. Figures 11(c) and (d) show that in the matrix phase, the change of the cumulative curve of the models at different SDT values is insignificant, and the average and maximum stresses slightly decrease with the increase of SDT values, which indicates that the matrix phase is insensitive to the increase of CR and on the contrary, the increase in CR may reduce the stress in the matrix. In Figures 11(e) and (f), it can be noticed that the volumetric ratio of the high stress and average stress in CR reduces with the increase of SDT values, which suggests that the CR with a smaller SDT has a more significant effect. Besides, it is noteworthy that the three phases' maximum stresses are almost the same for the virtual-specimen models at different SDT values, indicating that the SDT values cannot dramatically affect the continuous and uniform stress distribution characteristic in the virtual-specimen model.

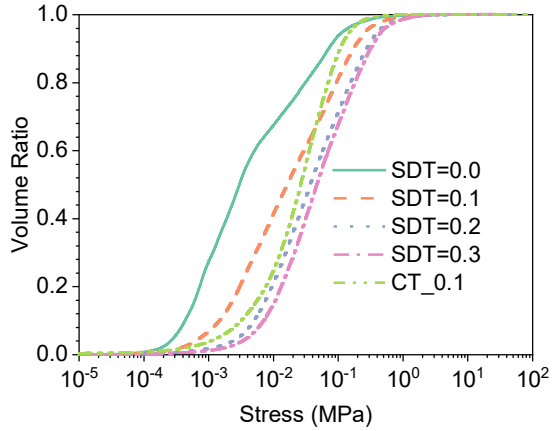


(a) Cumulative distribution curves of aggregate

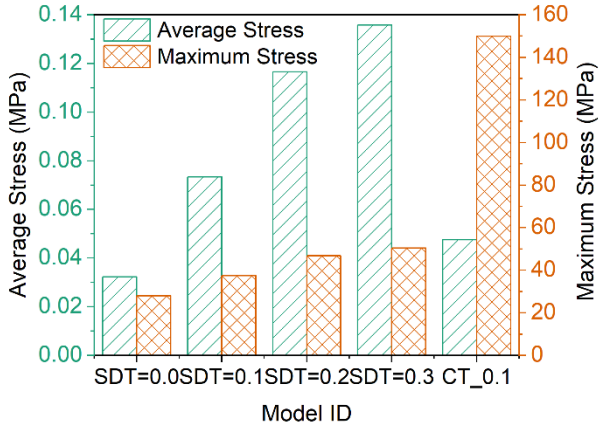


(b) Average and maximum stress of aggregate

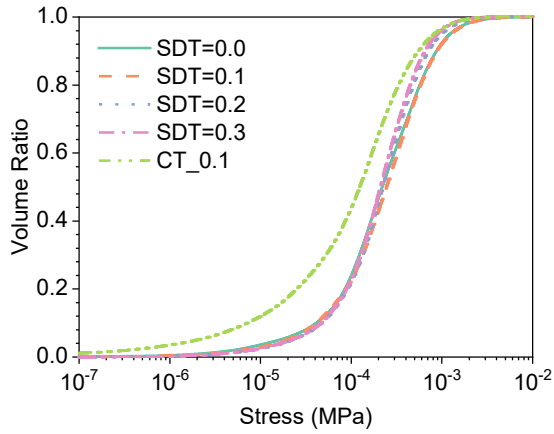


(c) Cumulative distribution curves of matrix

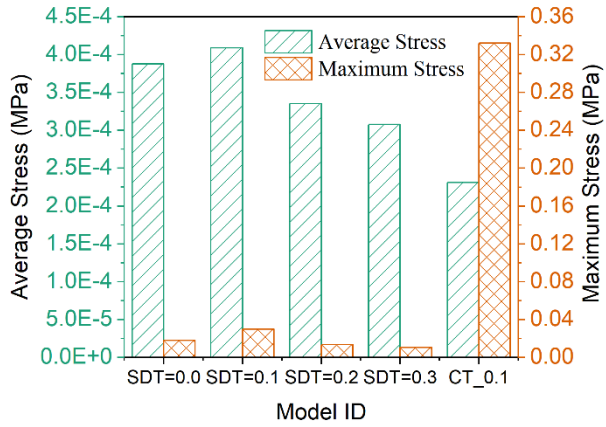


(d) Average and maximum stress of matrix

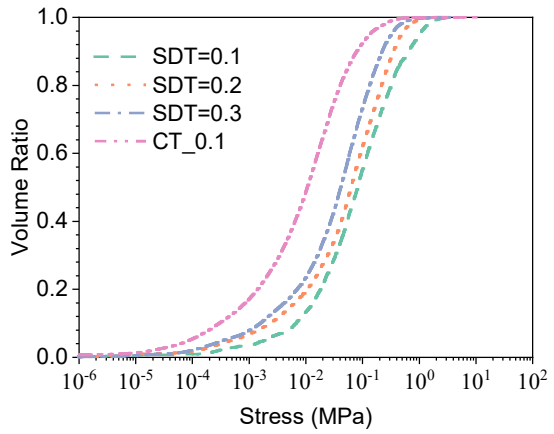


(e) Cumulative distribution curves of CR

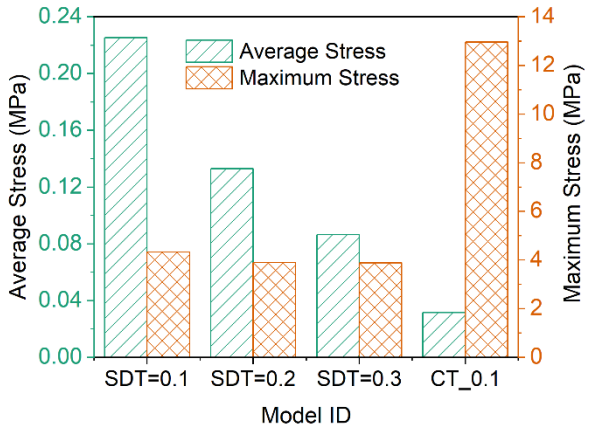


(f) Average and maximum stress of CR

Figure 11 Statistical analysis maximum principal stress properties of SMA10_1 model at different SDT values and SMA10_CT_0.1 model at $10^{-6}$ Hz

## 6 Findings and conclusions

This study proposes a virtual-specimen modeling method which can consider aggregate-to-aggregate contacts in asphalt concrete. The virtual-specimen models for a gap-graded mixture (SMA10) and a dense-graded mixture (AC10) are generated with different SDT values and applied to predict both mixtures' complex moduli in a broad frequency range. Besides, the stress distributions of the virtual-specimen models are statistically analyzed and compared with the CT image-based model. Moreover, the effects of SDT

values on the stress distributions of virtual-specimen models are evaluated. The following points summarize the main findings of this study:

- The virtual-specimen model with simplified aggregates can make the modeling more computationally efficient than the CT-based model. Compared with the CT image-based FE model, the proposed method can significantly reduce the number of elements in the generated FE model.
- The numerical model with aggregate contacts generated by the proposed method can predict the complex modulus of asphalt concrete with reasonable accuracy. The modeling results on both mixtures show that with a 0.2 mm SDT value of CR, the prediction accuracies of the master curves for both asphalt mixtures can be significantly improved, especially at the low-frequency range, using the experimental results as a reference. The virtual-specimen model of SMA10 provides almost identical master curves as the CT model.
- The virtual-specimen model generated by the proposed method has a more uniform and continuous stress distribution than the CT image-based model. Compared with the real irregular aggregates, the aggregate particles represented by spheres in the virtual-specimen model reduce the stress concentration in aggregate particles. This characteristic may be advantageous to the numerical computation but may also lose some local failure properties of asphalt concrete.
- Although the volumetric percentage of CR in asphalt concrete is tiny, it can significantly improve the stress transmission among contacting aggregates, thus increasing the moduli of asphalt concrete at low frequencies. Statistical analysis shows that the volumetric percentages of CR in both mixtures are low than 2%, but it can improve the dynamic moduli of SMA10 and AC10 at $10^{-6}$ Hz for more than ten times and one time, respectively.
- Aggregate contacts more significantly affect the gap-graded mixture than the dense-graded mixture. The stress distributions in the virtual-specimen models show that the CR in SMA10 exhibits higher stress than AC10 at low frequencies, indicating better stress transmission in SMA10 than AC10.

In conclusion, the proposed virtual-specimen generation approach provides a cost-effective and efficient way to create numerical models of asphalt concrete, which can consider the effects of aggregate-to-aggregate interaction. Such models can quantify the effect of volumetric composition change on asphalt mixtures' performance. In this study, the virtual-specimen modeling approach has been successfully applied to predict the complex moduli of different asphalt mixtures. In future research, the application of this approach for more purposes, such as evaluating the effect of aggregate contact network parameters on the damage resistance of asphalt concrete, will be further investigated.

# 7 References

[1] H. Zhu, J.E. Nodes, Contact based analysis of asphalt pavement with the effect of aggregate angularity, Mechanics of

Materials 32(3) (2000) 193-202.

[2] P. Li, J. Su, S. Ma, H. Dong, Effect of aggregate contact condition on skeleton stability in asphalt mixture, International Journal of Pavement Engineering 21(2) (2020) 196-202.

[3] J. Jiang, F. Ni, L. Gao, L. Yao, Effect of the contact structure characteristics on rutting performance in asphalt mixtures using 2D imaging analysis, Construction and Building Materials 136 (2017) 426-435.

[4] J. Jiang, F. Ni, Q. Dong, L. Yao, X. Ma, Investigation of the internal structure change of two-layer asphalt mixtures during the wheel tracking test based on 2D image analysis, Construction and Building Materials 209 (2019) 66-76.

[5] X. Shu, B. Huang, Dynamic modulus prediction of HMA mixtures based on the viscoelastic micromechanical model, Journal of Materials in Civil Engineering 20(8) (2008) 530-538.

[6] Y. Sun, J. Chen, B. Pan, X. Shu, B. Huang, Three-dimensional micromechanical complex-modulus prediction of asphalt concrete considering the aggregate interlocking effect, Journal of Materials in Civil Engineering 29(10) (2017) 04017153.

[7] H. Zhang, K. Anupam, A. Scarpas, C. Kasbergen, S. Erkens, Effect of stone-on-stone contact on porous asphalt mixes: Micromechanical analysis, International Journal of Pavement Engineering 21(8) (2020) 990-1001.

[8] E. Olsson, D. Jelagin, M.N. Partl, New discrete element framework for modelling asphalt compaction, Road Materials and Pavement Design 20(sup2) (2019) S604-S616.

[9] X. Yang, Z. You, C. Jin, A. Diab, M.R. Mohd Hasan, Aggregate morphology and internal structure for asphalt concrete: prestep of computer-generated microstructural models, International Journal of Geomechanics 18(10) (2018) 06018024.

[10] M.R. Pouranian, M. Shishehbor, J.E. Haddock, Impact of the coarse aggregate shape parameters on compaction characteristics of asphalt mixtures, Powder Technology 363 (2020) 369-386.

[11] F. Chen, D. Jelagin, M.N. Partl, Experimental and numerical analysis of asphalt flow in a slump test, Road Materials and Pavement Design 20(sup1) (2019) S446-S461.

[12] F. Chen, D. Jelagin, M.N. Partl, Vibration-induced aggregate segregation in asphalt mixtures, Materials and Structures 53(2) (2020) 1-14.

[13] C. Ling, H. Bahia, Modelling of aggregates' contact mechanics to study roles of binders and aggregates in asphalt mixtures rutting, Road Materials and Pavement Design 21(3) (2020) 720-736.

[14] Z. Tan, Z. Leng, J. Jiang, P. Cao, D. Jelagin, G. Li, A. Sreeram, Numerical study of the aggregate contact effect on the complex modulus of asphalt concrete, Materials & Design 213 (2022) 110342.

[15] A.R. Coenen, M.E. Kutay, N.R. Sefidmazgi, H.U. Bahia, Aggregate structure characterisation of asphalt mixtures using two-dimensional image analysis, Road Materials and Pavement Design 13(3) (2012) 433-454.

[16] M.E. Kutay, E. Arambula, N. Gibson, J. Youtcheff, Three-dimensional image processing methods to identify and characterise aggregates in compacted asphalt mixtures, International Journal of Pavement Engineering 11(6) (2010) 511-528.

[17] Q. Yu, H. Liu, T. Yang, H. Liu, 3D numerical study on fracture process of concrete with different ITZ properties using X-ray computerized tomography, International Journal of Solids 147 (2018) 204-222.

[18] P. Liu, J. Hu, D. Wang, M. Oeser, S. Alber, W. Ressel, G.C. Falla, Modelling and evaluation of aggregate morphology on asphalt compression behavior, Construction and Building Materials 133 (2017) 196-208.

[19] E. Coleri, J.T. Harvey, K. Yang, J.M.J.C. Boone, B. Materials, Development of a micromechanical finite element model from computed tomography images for shear modulus simulation of asphalt mixtures, 30 (2012) 783-793.

[20] K.Z. Rami, S. Amelian, Y.-R. Kim, T. You, D.N. Little, Modeling the 3D fracture-associated behavior of viscoelastic asphalt mixtures using 2D microstructures, Engineering Fracture Mechanics 182 (2017) 86-99.

[21] H. Fadil, D. Jelagin, P.-L. Larsson, M.N. Partl, Measurement of the viscoelastic properties of asphalt mortar and its components with indentation tests, Road Materials Pavement Design 20(sup2) (2019) S797-S811.

[22] H. Fadil, D. Jelagin, M.N. Partl, A new viscoelastic micromechanical model for bitumen-filler mastic, Construction and Building Materials 253 (2020) 119062.

[23] B.S. Underwood, Y.R. Kim, Microstructural investigation of asphalt concrete for performing multiscale experimental studies, International Journal of Pavement Engineering 14(5) (2013) 498-516.

[24] T. You, Y.-R. Kim, K.Z. Rami, D.N. Little, Multiscale modeling of asphaltic pavements: Comparison with field performance and parametric analysis of design variables, Journal of Transportation Engineering, Part B: Pavements 144(2) (2018) 04018012.

[25] Y. Sun, C. Du, C. Zhou, X. Zhu, J. Chen, Analysis of load-induced top-down cracking initiation in asphalt pavements using a two-dimensional microstructure-based multiscale finite element method, Engineering Fracture Mechanics 216 (2019) 106497.

[26] C. Du, G. Lu, H. Wang, Y. Sun, P. Liu, D. Wang, S. Leischner, M. Oeser, Effect of filler on performance of porous asphalt pavement using multiscale finite element method, International Journal of Pavement Engineering (2021) 1-11.

[27] B. Underwood, Multiscale Constitutive Modeling of Asphalt Concrete, (2011).

[28] Y. Zhang, Z. Leng, Quantification of bituminous mortar ageing and its application in ravelling evaluation of porous asphalt wearing courses, Materials & Design 119 (2017) 1-11.

[29] N.W. Tschoegl, The phenomenological theory of linear viscoelastic behavior: an introduction, Springer Science & Business Media1989.

[30] I. Onifade, D. Jelagin, A. Guarin, B. Birgisson, N. Kringos, Asphalt Internal Structure Characterization with X-Ray Computed Tomography and Digital Image Processing, Springer Netherlands, Dordrecht, 2013, pp. 139-158.

[31] S. Hang, TetGen, a Delaunay-based quality tetrahedral mesh generator, ACM Trans. Math. Softw 41(2) (2015) 11.

[32] Z. Leng, Z. Tan, P. Cao, Y. Zhang, An efficient model for predicting the dynamic performance of fine aggregate matrix, Computer-Aided Civil

Infrastructure Engineering 36 (2021) 1467-1479.

[33] P. Cao, F. Jin, C. Zhou, D. Feng, W. Song, Steady-state dynamic method: An efficient and effective way to predict dynamic modulus of asphalt concrete, Construction and Building Materials 111 (2016) 54-62.

[34] R.M. Huurman, L. Mo, M.F. Woldekidan, Unravelling porous asphalt concrete towards a mechanistic material design tool, Road Materials and Pavement Design 11(3) (2010) 583-612.